Dynamic and Degradable Imine-Based Networks for 3D-Printing of Soft Elastomeric Self-Healable Devices

Mathilde Grosjean, Lucien Guth, Stéphane Déjean, Cédric Paniagua, Benjamin Nottelet

ADVANCED MATERIALS INTERFACES
Open Access
www.advmatinterfaces.de

Dynamic and Degradable Imine-Based Networks for 3D-Printing of Soft Elastomeric Self-Healable Devices

*Mathilde Grosjean, Lucien Guth, Stéphane Déjean, Cédric Paniagua, and Benjamin Nottelet**

Self-healable degradable networks encounter a growing popularity for biomedical applications due to their ability to recover their properties after damage. Self-healable hydrogels dominate with applications in tissue engineering and drug delivery. On the opposite and despite their potential for medical devices, self-healable elastomers remain scarce, especially if they must be compatible with fused deposition modeling (FDM) 3D-printing and self-heal at physiological temperature under a hydrated state. These unmet challenges are addressed in this work with degradable elastomeric networks based on dynamic imine bonds prepared from multi(aldehyde) and multi(amine) hydrophobic PEG-PLA star-shaped copolymers. The star topology of these copolymers is the key feature of the strategy as it allows the design of multifunctional high molecular weights pre-polymers that ensure an efficient dynamic chemical crosslinking while guaranteeing access to the FDM process generally restricted to thermoplastics. The proposed elastomeric networks combine high self-healing efficiencies at 37 °C (>97%) with mechanical properties compatible with soft tissues and a linear degradation profile. Their FDM processing to produce self-healable tubular devices is demonstrated. Finally, their cytocompatibility is assessed and confirm their potential as biodegradable elastomeric networks to be used for the design of self-healable 3D-printed devices for biomedical applications.

1. Introduction

Degradable 3D polymer networks with the capacity to withstand significant deformation and stress while recovering their initial structure at rest are of particular interest for tissue engineering applications as they display mechanical behavior compatible with soft tissues.[1–3] Moreover, degradable chemically crosslinked networks preserve their 3D structure over degradation and therefore lose their mechanical properties homogeneously in time. However, they cannot be healed after accidental damage or breaking (cracking, cutting, stretching) caused by user manipulation, surgical handling, or implementation,[4] and cannot be remodeled to cope with surgical requirements or operative techniques. Therefore, self-healable networks have recently encountered a growing popularity.[4–9] Different strategies are encountered to provide self-healing properties to macromolecular networks depending on the nature of the bonds, either dynamic physical bonds (eg. hydrophobic interactions, hydrogen bonds, electrostatic interaction, metal-ligand interaction, host-guest interaction and π–π stacking) or chemical reversible bonds (eg. Diels-Alder adducts, imine bonds, disulfide bonds, boronate ester bonds, and hydrazone bonds). Such strategies have been applied to degradable hydrogels with numerous examples reported in the literature. However, despite their strong potential for medical devices, those reporting degradable self-healable elastomers remain rare, especially if they must be compatible with the popular fused deposition modeling (FDM) 3D-printing.[10]

The systems describing degradable elastomers with self-healing properties often take advantage of the 2-ureido-1[1H]-pyrimidinone (UPy) group, which is a self-complementary quadruple hydrogen bonding unit with high dimerization constant.[11–15] For instance, elastomers based on supramolecular assembly of UPy functional PLA-PEG-PLA and able to self-heal in 270 s at 37 °C were prepared by Ren et al.[12] In another example UPy-grafted poly(tetramethylene ether) glycol and 4-arm star-shaped PCL have been used to design slow self-healing systems that could recover in 48 h at 40 °C.[13] Hydrogen bonds can also be used to confer self-healing properties without relying on UPy groups as it is the case in the example of Zhang et al. in which a self-healable alternating polyester-co-polyurethane was prepared based on the H-bonds of urethane groups.[16] In addition, our group also recently reported dual-crosslinked degradable elastomeric networks with fast self-healing properties at 37 °C, based on the dynamic dissociation/reassociation

M. Grosjean, L. Guth, S. Déjean, C. Paniagua, B. Nottelet
Polymers for Health and Biomaterials
IBMM
Univ Montpellier
CNRS
ENSCM
Montpellier, France
E-mail: benjamin.nottelet@umontpellier.fr

The ORCID identification number(s) for the author(s) of this article can be found under https://doi.org/10.1002/admi.202300066.

DOI: 10.1002/admi.202300066

of hydrogen bonds between catechol groups.[17] Supramolecular ionic interactions were also used to design degradable self-healable elastomers.[18] In this case, a PCL diol was modified with isophorone diisocyanate (IPDI) before chain extension with anionic oligo-alginate or cationic N-methyldiethanolamine, leading to polyurethanes (PU) with ionic interaction among the PU chains. Coming to dynamic chemical bonds, elastomers based on disulfide bonds are the most common.[19,20] For example, elastomers able to self-heal in 2 h at 30 °C were prepared via polycondensation of dicarboxylic acids, 1,4-butanediol, glycerol and 3,3′-dithiopropionic acid. Some self-healable systems also rely on dynamic oxime-urethane bonds, that can be hydrolyzed.[21] For example, Jiang et al. designed biodegradable and biocompatible elastomers from dimethylglyoxime, polytetramethylene ether glycol, IPDI, and glycerol able to almost quantitatively recover their mechanical properties in 5 min at room temperature.[22] Other works described elastomers based on Diels-Alder reaction and prepared by reacting furan and maleimide functional PCL.[23,24] However, in this case, the self-healing was limited, and only partial healing was achieved. Finally, You et al. used heat-triggered transesterification to prepare self-healing poly(sebacoyldiglyceride-co-4,4′-azodibenzoyl diglyceride) elastomers based on the light-to-heat conversion ability of the azobenzene moieties.[25]

The Schiff-base dynamic crosslinking appears as a powerful and widely used approach to designing self-healing hydrogels.[10] Indeed, imines are involved in various reversible reactions[26] as described in **Figure 1** (hydrolysis/condensation, transamination, imine metathesis) that can all be involved in the self-healing process. However, this strategy is in its infancy when it comes to elastomers. The use of imine bonds was reported by Li et al. [27] who combined terephtaldehyde with various diamines and tri(2-aminoethyl)amine to lead elastomers with the ability to heal at temperatures ranging from 20 to 55 °C.

In this work, we design degradable elastomeric networks based on dynamic imine bonds that combine high mechanical properties, linear degradation, and self-healing abilities, while being compatible with 3D-printing. To this end, a degradable 8-arm star-shaped PEG-*b*-PLA (PEG_{s8}-PLA) block copolymer is prepared and used as a building block of the system through its functionalization with aldehyde or amine groups to yield multi(aldehyde) star-shaped PEG_{8arm}10k-*b*-PLA (PEG_{s8}-PLA-AL) and multi(amine) star-shaped PEG_{8arm}10k-*b*-PLA (PEG_{s8}-PLA-AM). The star topology of these copolymers is the key feature of our strategy as it allows the design of multifunctional high molecular weights pre-polymers that ensure an efficient dynamic chemical crosslinking while guaranteeing access to the FDM process that is generally restricted to thermoplastics. Degradable crosslinked networks are then formulated by mixing the two complementary copolymers. The mechanical properties, the self-healing abilities at 37 °C, the biodegradability, and the cytotoxicity are investigated and discussed. Finally, the material is processed by FDM 3D-printing to produce self-healable tubular devices.

2. Experimental Section

2.1. Materials

Hydroxyl-terminated eight-armed poly(ethylene glycol) (tripentaerythritol) (PEG_{8arm}10k, Mw = 10 000 g mol^{-1}) was purchased from JenKem Technology Co., Ltd (Beijing, China). D,L-lactide was purchased from Corbion (Gorinchem, The Netherlands). Tin(II) 2-ethylhexanoate ($Sn(Oct)_2$), dichloromethane (DCM), N,N′-dicyclohexylcarbodiimide (DCC), 4-dimethylaminopyridine (DMAP), 4-formylbenzoic acid, 4-aminobenzoic acid, Celite 545, ethanol (EtOH), tetrahydrofuran (THF) were purchased from Sigma-Aldrich (St Quentin Fallavier, France). All chemicals were used without further purification with exception of DCM which was dried over calcium hydride and freshly distillated before use.

2.2. Characterization

Average molecular weights ($\overline{Mn}$) and dispersities (Đ) were determined by size exclusion chromatography (SEC, Shimadzu SIL-20A HT) using two mixed medium columns PLgel 5 µm MIXED-C (300 × 7.8 mm), a Shimadzu RI detector 20-A and

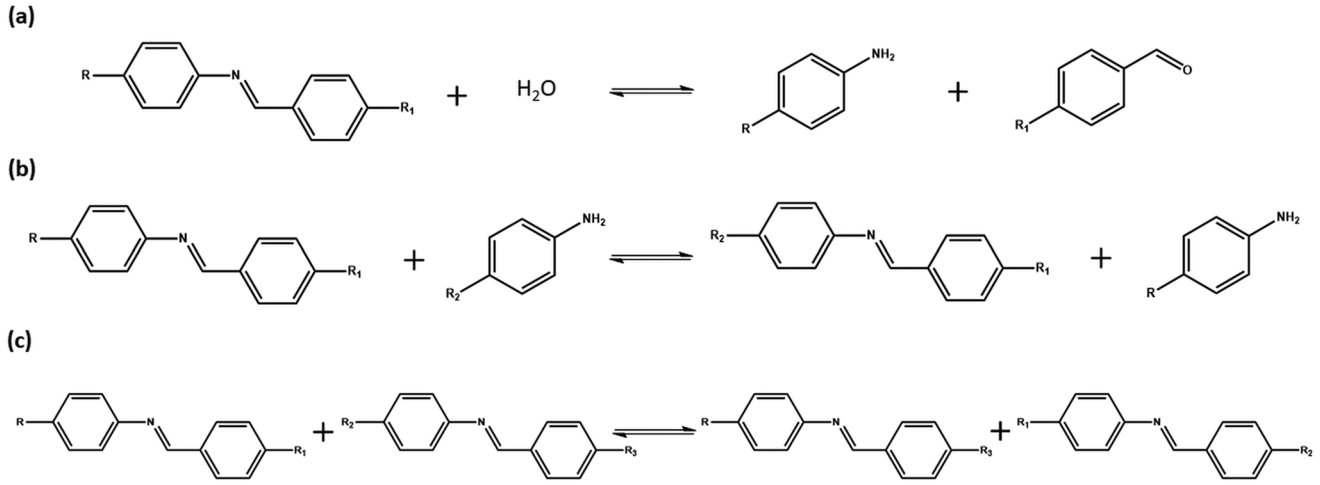

Figure 1. Reversible reactions involving imines: a) hydrolysis/condensation, b) transimination, and c) imine metathesis.

a Shimadzu UV detector SPD-20A (260 and 290 nm) (40 °C thermostatic analysis cells). THF was the mobile phase with 1 mL.min^{-1} flow at 30 °C (column temperature). Polymer was dissolved in THF to reach 5 mg mL^{-1} concentration. Afterward, solution was filtered through a 0.45-µm Millipore filter before being injected. $\overline{Mn}$ and Đ were expressed according to calibration using polystyrene standards.

^{1}H nuclear magnetic resonance (NMR) spectra were recorded using a Bruker Avance III HD spectrometer operating at 400 MHz at room temperature. ^{1}H 2D diffusion-ordered (DOSY) NMR spectra were recorded using a Bruker Avance III spectrometer operating at 600 MHz at room temperature. The solvent used was deuterated chloroform or deuterated dimethylsulfoxide. The chemical shift was expressed in ppm with respect to tetramethylsilane.

Differential scanning calorimetry (DSC) analyses were performed using a Mettler Toledo DSC 3 STAR System instrument, under nitrogen atmosphere. Samples were placed in a perforated aluminum pan and heated from 0 °C to 100 °C (10 °C min^{-1}), then cooled to –80 °C (10 °C min^{-1}), and heated again to 200 °C (5 °C min^{-1}). The melting temperature (*T*m) or glass transition temperature (*T*g) were measured on the second heating ramp.

Thermogravimetric analyses (TGA) were carried out using a Mettler Toledo TGA 2 STAR System instrument, under nitrogen atmosphere. Samples were placed in an aluminum crucible and heated from room temperature (≈25 °C) to 400 °C at a heating rate of 5 °C min^{-1}.

Fourier-transform infrared spectroscopy (FTIR) spectra were recorded using a Perkin Elmer Spectrum 100 spectrometer.

2.3. Synthesis of Copolymers

Star-shaped copolymer $PEG_{8arm}10k\text{-}(PLA_{69})_8$ (PEG_{s8}-PLA) was synthesized according to the procedure recently reported by our group.[28] Synthetic details are given in the supporting information (Appendix S2, Supporting Information).

2.3.1. Benzaldehyde Functional Copolymer PEG_{s8}-PLA-AL

The 8-armed star block copolymer PEG_{s8}-PLA was solubilized in DCM (10% w/v). Determined amounts (2.5 eq./OH group) of DCC, DMAP and 4-formylbenzoic acid were added. The mixture was then heated at 40 °C for 72 h under stirring. Then, the reaction medium was filtered on Celite 545 before being washed with distilled water and concentrated. Afterward, the mixture was precipitated in cold EtOH. The benzaldehyde functional $PEG_{8arm}10k\text{-}(PLA_{69})_8$-AL ($PEG_{s8}$-PLA-AL) was dried under reduced pressure to constant mass.

The functionalization was confirmed by ^{1}H NMR and DOSY-NMR.

The yield of functionalization was determined by comparing the integration of the signal at 10.1 ppm characteristic of aldehyde and the integration of proton resonance at 3.5 ppm characteristic of methylene groups of PEG chains.

^{1}H NMR (400 MHz; DMSO-d_6): δ (ppm) = 10.1 (s, 1H, C = CH = CH = C-CO***H***), 8.2 (m, 2H aromatic ring, C = C***H*** = CH = C-COH), 8.1 (m, 2H aromatic ring, C = CH = C*H* = C-COH), 5.2 (q, 1H, CO-C***H***-(CH_3)-O), 4.2 (m, 2H, O-CH_2-C-C***H$_2$***-O), 3.5 (s, 4H, C***H$_2$***-C***H$_2$***-O), 3.3 (m, 2H, O-C***H$_2$***-C-CH_2-O), 1.5 (t, 3H, CO-CH-(C***H$_3$***)-O).

2.3.2. Phenylamine Functional Copolymer PEG_{s8}-PLA-AM

The 8-armed star block copolymer PEG_{s8}-PLA was solubilized in DCM (10% w/v). Determined amounts (5 eq./OH group) of DCC, DMAP, and 4-aminobenzoic acid were added. The mixture was then heated at 40 °C for 5 days under stirring. Then, the reaction medium was filtered on Celite 545 before being washed with distilled water and concentrated. Afterward, the mixture was precipitated in cold EtOH. The phenylamine functional $PEG_{8arm}10k\text{-}(PLA_{69})_8$-AM ($PEG_{s8}$-PLA-AM) was dried under reduced pressure to constant mass.

The functionalization was confirmed by ^{1}H NMR and DOSY-NMR.

The yield of functionalization was determined by comparing the integration of the signal at 7.6, 6.5, and 6.1 ppm characteristic of phenylamine, and the integration of proton resonance at 3.5 ppm characteristic of methylene groups of PEG chains.

^{1}H NMR (400 MHz; DMSO-d_6): δ (ppm) = 7.6 (m, 2H aromatic ring, C = C***H*** = CH = C-NH_2), 6.5 (m, 2H aromatic ring, C = CH = C***H*** = C-NH_2), 6.1 (s, 2H, C = CH = CH = C-N***H$_2$***), 5.2 (q, 1H, CO-C***H***-(CH_3)-O), 4.2 (m, 2H, O-CH_2-C-CH_2-O), 3.5 (s, 4H, C***H$_2$***-C***H$_2$***-O), 3.3 (m, 2H, O-C***H$_2$***-C-CH_2-O), 1.5 (t, 3H, CO-CH-(C***H$_3$***)-O).

2.4. Film Preparation, Crosslinking, and Gel Fraction

Polymer films were prepared using the solvent casting technique. The copolymers were first solubilized in DCM (10% w/v) at a 1:1 aldehyde/amine ratio. Then, the solutions were slowly dried in a mold to obtain thin films (thickness ≈300 µm), which were further dried under vacuum for 24 h.

The resulting films were crosslinked under vacuum in an oven at 80 °C for 24 h.

Afterward, samples were cut (10 × 10 mm) and weighed before being placed in DCM (5 mL) under stirring. After 24 hours, the insoluble crosslinked parts were removed from DCM, dried under vacuum, and weighed to determine the gel fraction according to Equation (1). The experiment was run in triplicate.

$$\text{Gel fraction}\,(\%) = \frac{\text{Weight of insoluble crosslinked parts}}{\text{Weight of initial sample}} \times 100 \qquad (1)$$

2.5. Water Uptake

Samples were cut (10 × 10 mm) and weighed (Wi = initial weight) before being placed in 5 mL of phosphate buffer saline (PBS) (pH 7.4) at 37 °C under stirring. At different time points, samples were removed from PBS and weighed (*W*w = weight of the wet samples after w time in PBS) to determine the water uptake from Equation (2). The experiment was run in triplicate.

$$\text{Water uptake}\,(\%) = \frac{Ww - Wi}{Wi} \times 100 \quad (2)$$

2.6. Mechanical Properties

Tensile tests: The mechanical properties were assessed at room temperature on dog-bone strips (10 × 2 mm) stamped from polymer films with an Instron 3344 testing machine equipped with a 500 N load cell at a deformation rate of 10 mm min^{-1}.

Tensile properties were also evaluated in hydrated state. Samples were hydrated for 2 h before the tensile tests and were tested on the same testing machine equipped with the BioPuls Bath accessory, at 37 °C in deionized water.

Young's modulus (E, MPa), stress at yield (σ_{yield}, MPa), strain at yield (ε_{yield}, %), stress at break (σ_{break}, MPa), and strain at break (ε_{break}, %), were expressed as the mean value of three measurements.

Cyclic loads (tensile mode): The samples were subjected to 9 cycles during which they were elongated to 15% and subsequently let to recover (0%) before immediately being stretched again to 15%. The resilience was calculated according to Equation (3) from the value of the ninth cycle to evaluate the capacity of the material to deform reversibly without loss of energy. Same tests were repeated with deformation of 5 and 2%.

$$\text{Resilience}\,(\%) = \frac{\text{Area under unloading curve}}{\text{Area under loading curve}} \times 100 \quad (3)$$

Resilience (%) was expressed as the mean of three measurements.

Relaxation (tensile mode): The samples were elongated to 15% and the strength needed to maintain the constant elongation was monitored for 800 s The relaxation was calculated according to Equation (4) to evaluate the ability of the material to release the mechanical stress under constant deformation. Same tests were repeated with deformation of 10, 5, and 2%.

$$\text{Relaxation}\,(\%) = \frac{\text{Initial strength}}{\text{Final strength}} \times 100 \quad (4)$$

Relaxation (%) was expressed as the mean of three measurements.

Compression tests: Compression tests under constant deflection were carried out with an Instron 3344 testing machine equipped with 10 kN compression platens and a 500 N load cell. After measuring the initial height (H_0), the tubular samples (1 cm in diameter and height) were compressed at 25% strain for 10 minutes (H_n). Then, samples were allowed to recover at room temperature for 30 min, and sample height was measured (H_{30}). The compression set, which corresponds to the permanent deformation remaining after the removal of the force applied to the material, was calculated according to Equation (5). Same tests were repeated with deformation of 15%.

$$\text{Compression set}\,(\%) = \frac{H_0 - H_{30}}{H_0 - H_n} \times 100 \quad (5)$$

Compression set (%) was expressed as the mean of three measurements.

Cyclic loads (compression mode): The tubular samples (1 cm in diameter and height) were compressed at 15% strain and subsequently let to recover (0%) before immediately being compressed again to 15% (nine cycles). To evaluate the ability of the material to deform reversibly without loss of energy, the resilience was calculated according to Equation (3). It was calculated from the value of the ninth cycle. Same tests were repeated with deformation of 5 and 2%.

Resilience (%) was expressed as the mean of three measurements.

Dynamic mechanical analysis (DMA): Dynamic mechanical analyses (DMA) were carried out on rectangle specimens (10 × 3 mm) in tensile mode using a Mettler Toledo DMA 1 Star System with temperature scans from –60 °C to 60 °C, at a frequency of 1 Hz with a fixed strain of 0.1% and a preload of 1N. The heating rate was 2 °C min^{-1}. The storage modulus (E'), and the loss modulus (E'') are expressed in MPa and tan δ is dimensionless according to Equation (6). Tα was determined as the temperature for which the value of E'' is maximum.

$$\tan\delta = \frac{E'}{E''} \quad (6)$$

2.7. Self-Healing Study

The self-healing was studied using the overlap method. Dog-bone strips were stamped from polymer films (thickness of ≈300 µm) before being cut into two pieces using a razor blade. The pieces were then slightly overlapped (contact area = 1 mm^2), pressed for 5 s, and heated at 37 °C in an oven for different times (5, 15, 30, 60, and 120 min).

The mechanical properties of the healed dog-bone samples were tested 10 min after removal from the oven and the mechanical self-healing efficiency (SHE) was evaluated as the ratio between the restored stress and strain at break (*ie.* after self-healing) to the original stress and strain at break (ie. before the cut) – Equation (7) and (8).

$$\text{SHE}_\sigma\,(\%) = \frac{\text{restored } \sigma_{break}}{\text{original } \sigma_{break}} \times 100 \quad (7)$$

$$\text{SHE}_\varepsilon\,(\%) = \frac{\text{restored } \varepsilon_{break}}{\text{original } \varepsilon_{break}} \times 100 \quad (8)$$

The self-healing properties were also evaluated in hydrated state. The same protocol as before was used except that the samples were immersed in PBS before being heated at 37 °C for 120 min in an oven and tested using the BioPuls bath accessory as described in Section 2.6. The SHE was calculated using the original stress and strain at break in hydrated state at 37 °C.

2.8. 3D-Printing

The benzaldehyde and phenylamine functional copolymers were stirred in DCM at a 1:1 aldehyde/amine ratio (10% w/v).

The mixture was then dried under vacuum and ground using a Retsch ZM 200 crusher to yield powder.

The 3D-printing was then performed using a 3D-Bioplotter EnvisionTEC system. The powder was introduced in a metal cartridge assembly for high-temperature head fitted with a 480 µm inner diameter needle. The printing was carried out at 80 °C with a pressure of 4 bar and a speed of 1 mm s^{-1}.

Tubes of 1 cm in diameter and height were printed. In order to maintain their shape during the crosslinking step, the tubes were placed around a glass rod covered with Teflon sheet before being heated at 80 °C under a vacuum for 24 h.

2.9. Degradation Study

Samples were cut (10 × 10 mm), weighed (Wi = initial weight), and placed in 5 mL of PBS (pH 7.4) at 37 °C under stirring. At different time points, samples were removed from PBS before being rinsed and dried to constant mass (Wx = dry weight after x time in PBS). The remaining mass of the samples was calculated from Equation (9). The experiment was run in triplicate.

$$\text{Remaining mass}\,(\%) = \frac{Wx}{Wi} \times 100 \tag{9}$$

2.10. Cytocompatibility Evaluation

Cells and control polymer films were chosen following ISO 10993–5 guidelines. Mouse fibroblasts L929 cells (ECACC 85 011 425) were maintained in DMEM high glucose supplemented with 5% Fetal Bovine Serum, 1% L-glutamine, and 1% penicillin/streptomycin and cultured at 37 °C and 5% CO_2. Cells were tested to be free of mycoplasms. Negative (RM-C High-Density Polyethylene noted C-) and positive (RM-B 0.25% Zinc Dibutyldithiocarbamate polyurethane, noted C+) control films were purchased from Hatano Research Institute (Ochiai 729-5, Hadanoshi, Kanagawa 257, Japan).

Cytotoxicity was first assessed on extracts. Extractions were carried out at 6 cm^2 of polymer film per mL for 24 h at 37 °C under sterile conditions in a complete growth medium following ISO 10993-12 recommendations. Films were irradiated under UV-light for 5 min. L929 cells were seeded at 10 × 10^3 cells per well in a 96-well plate and allowed to attach overnight. The culture medium was then removed and discarded from the cultures and an aliquot of the polymer extract was added to each well. After 24 h of incubation, extract cytotoxicity was assessed using the CellTiter-Glo Luminscent Cell Viability Assay, according to the manufacturer's instruction. Briefly, 50 µL medium from the well were removed and followed by the addition of the same volume of CellTiter-Glo. After 10 min of incubation at room temperature, luminescence was measured using a CLARIOstar microplate-reader (BMG LABTECH's) to quantify the ATP present.

Then, L929 cell proliferation on polymer films was evaluated over 7 days. Crosslinked films were cut in square samples of 1.6 × 1.6 cm (n = 4). The samples were then decontaminated under UV-light for 5 min and fixed in 24-well plates (TCPS non-treated for cell culture) using O-rings. L929 cells were seeded on top of the samples at 80 × 10^3 cells per well and placed at 37 °C and 5% CO_2. The number of cells was assessed after 1, 3, and 7 days of contact with the polymer films using a PrestoBlue assay that evaluates the transformation of weakly-fluorescent blue resazurin into highly fluorescent red resorufin through the mitochondrial activity of the cell. Briefly, the culture medium was removed, and the reagent was placed in each well a at ratio of 1:10 in culture medium and incubated in the dark for 40 min. Fluorescence intensity was then read using a Varioskan LUX (ThermoFisher SCIENTIFIC) microplate reader (wavelength: excitation 558 nm, emission 593 nm). After each measurement, the supernatant was replaced with fresh medium culture to continue the cell culture.

2.11. Statistical Analysis

OriginPro 2021 was used to perform statistical analysis. Significance was assessed by one-way ANOVA followed by Tukey test. Values of $^*p < 0.05$ were considered as statistically significant.

3. Results and Discussion

In this work, the final objective was to design chemically crosslinked degradable networks with self-healing properties. We chose to combine aldehyde and amine groups to produce crosslinked materials via the formation of imine bonds. Indeed, imine bonds – also called Schiff base – are known to be dynamic and are commonly used in the preparation of self-healing materials,[10] but to the best of our knowledge only one example of degradable imine-based elastomer was reported to date.[27] With aim to prepare such elastomers, our strategy consists in mixing multi(aldehyde) star-shaped PEG_{s8}-PLA-AL copolymer with multi(amine) star-shaped PEG_{s8}-PLA-AM. 8-arm PEG_{s8}-PLA copolymers were selected to increase the number of reactive sites per molecules, in order to reach high crosslinking efficiency and mechanical properties.

3.1. Synthesis of Benzaldehyde and Phenylamine Functional Copolymers

First, PEG_{s8}-PLA was synthesized by classical ROP procedures.[28] The molecular weight calculated by ^{1}H NMR agreed with the targeted one and a low dispersity below 1.2 was confirmed by SEC analysis (**Table 1**).

The nonfunctional star-shaped block copolymer PEG_{s8}-PLA was then reacted with 4-formylbenzoic acid to yield multi(aldehyde) star-shaped PEG_{s8}-PLA-AL (**Figure 2**a). The experimental molecular weight, the monomodal distribution, and the low dispersity of 1.2 determined by SEC analysis highlighted that no degradation of the copolymer occurred at this step (Table 1). A typical ^{1}H NMR spectrum of PEG_{s8}-PLA-AL copolymer is shown in Figure 2b. The peak at 10.1 ppm (peak a) corresponds to the characteristic proton of aldehyde group, whereas peaks at 8.2 and 8.1 ppm (peaks b and c) were attributed to aromatic protons of the benzaldehyde chain-ends. The peaks at 5.2 ppm (peak d) and 1.5 ppm (peak e) correspond

Table 1. Molecular weight, dispersity, and thermal properties of the star-shaped copolymers.

Copolymer	$\overline{Mn}_{NMR}$ [g mol^{-1}]	Đ	*Tg* [°C]	*Tm* [°C]
$PEG_{8arm}10k\text{-}(PLA_{69})_8$	51 400	1.2	12.8	nd[a)]
$PEG_{8arm}10k\text{-}(PLA_{69})_8$-AL	51 600	1.2	14.7	nd
$PEG_{8arm}10k\text{-}(PLA_{69})_8$-AM	52 300	1.2	13.3	nd

[a)]Not detected under the condition of analysis.

to the methine and methylene groups of the PLA backbone, respectively. The peaks at 4.2 ppm (peak g) were attributed to the tripentaerythritol core of the copolymers. Finally, the peak at 3.5 ppm (peak f) was assigned to the methylene groups of PEG. By comparison between the integration of the peaks of the methylene groups of PEG and of the benzaldehyde chain-ends, a functionalization degree of 100% was calculated. The grafting of benzaldehyde groups was further confirmed by ^{1}H DOSY NMR since benzaldehyde and copolymers signals had the same coefficient of diffusion (Figure S2, Supporting Information). Moreover, the appearance of a characteristic benzaldehyde UV signal (280 nm) on SEC analysis also confirmed the success of the grafting (Figure 2c).

The same strategy was followed to prepare phenylamine-functional polymers. The nonfunctional star-shaped block copolymer PEG_{s8}-PLA was reacted with 4-aminobenzoic acid to obtain multi(amine) star-shaped PEG_{s8}-PLA- AM (Figure 2d). The low dispersity below 1.2, the monomodal distribution determined by SEC analysis, and the experimental molecular weight calculated from ^{1}H NMR spectra confirmed that no degradation occurred at this step (Table 1). A typical ^{1}H NMR spectrum of PEG_{s8}-PLA-AM is shown in Figure 2e. Peaks at 7.6 and 6.5 ppm (peaks c and b) correspond to aromatic protons of the phenylamine chain-ends, whereas the peak at 6.1 ppm (peak a)

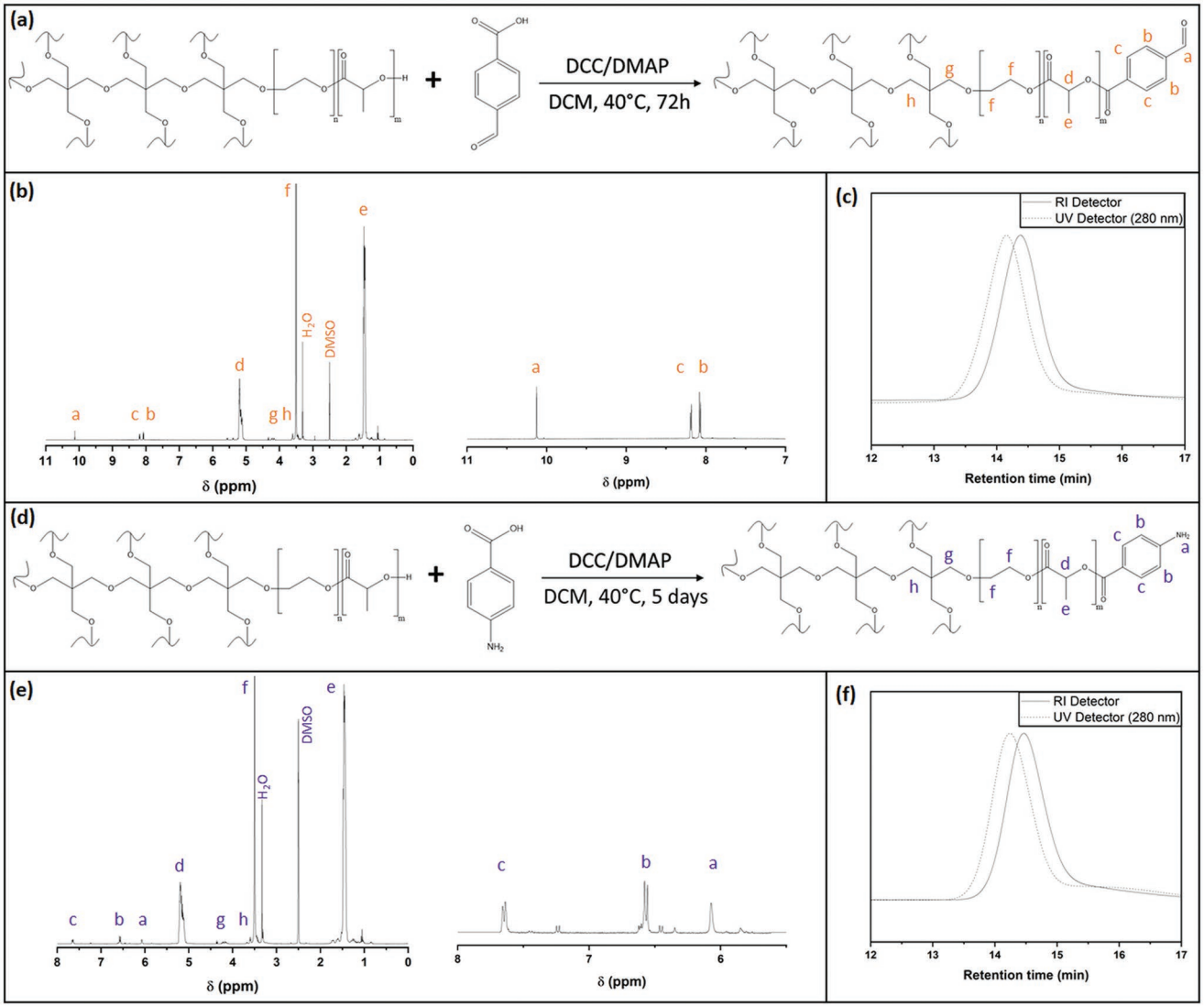

Figure 2. Synthesis and characterization of (multi)aldehyde functional star-shaped PEG_{s8}-PLA-AL and (multi)amine functional star-shaped PEG_{s8}-PLA-AM. a) Synthesis scheme of PEG_{s8}-PLA-AL. b) ^{1}H NMR spectrum of PEG_{s8}-PLA-AL. c) SEC analysis of PEG_{s8}-PLA-AL (refractive index and UV detection). d) Synthesis scheme of PEG_{s8}-PLA-AM. e) ^{1}H NMR spectrum of PEG_{s8}-PLA-AM. f) SEC analysis of PEG_{s8}-PLA-AM (refractive index and UV detection).

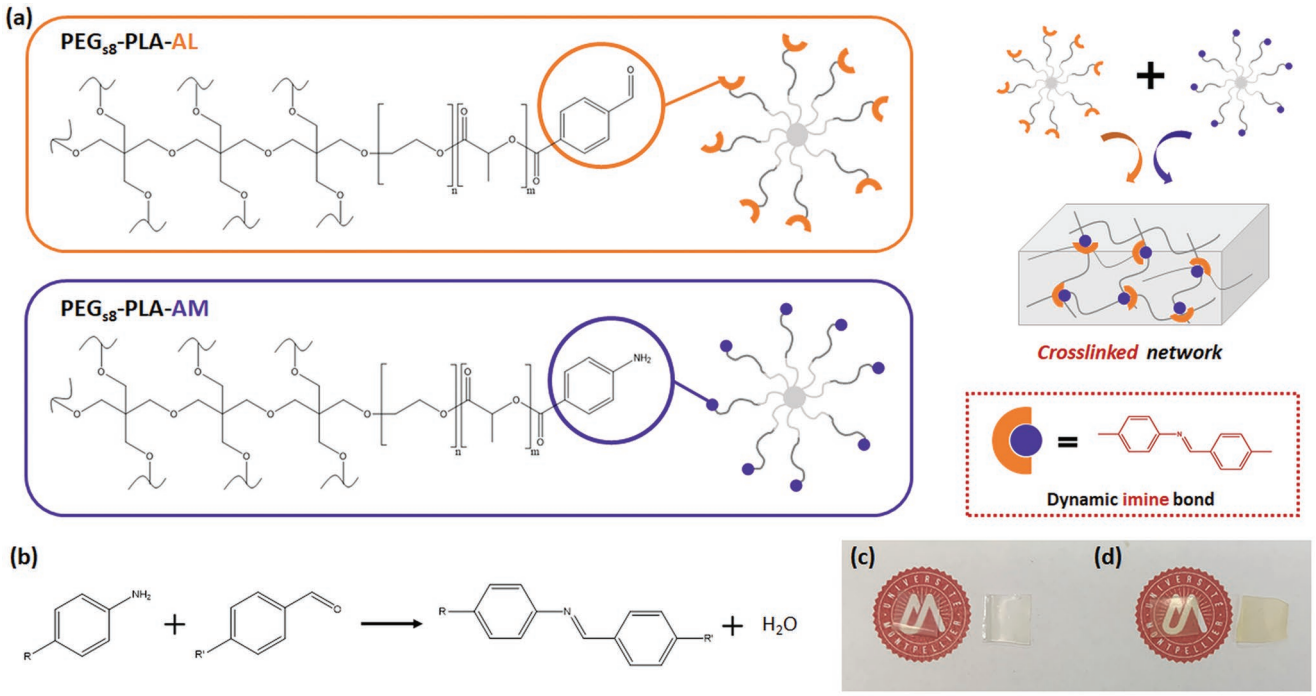

Figure 3. a) Chemical structures of multi(aldehyde) PEG$_{s8}$-PLA-AL and multi(amine) PEG$_{s8}$-PLA-AM mixed to generate crosslinked self-healable and degradable networks based on imine bonds. b) Crosslinking reaction. Picture of the film c) before and d) after cross-linking.

was assigned to the NH_2. As described previously, the other peaks correspond to the star-shaped PEG$_{s8}$-PLA. By comparison between the integration of the methylene groups of PEG and the phenylamine chain-ends, a functionalization degree of 90% was calculated. As shown in Figure 2f, the grafting of phenylamine functions was also confirmed by the appearance of UV signal (280 nm) on SEC analysis. Finally, ^{1}H DOSY NMR further confirmed the success of grafting with copolymers and phenylamine signals having the same coefficient of diffusion (Figure S3).

Overall, these results confirm the successful synthesis of aldehyde- or amine-functional star-shaped PEG-PLA.

3.2. Preparation of Crosslinked Networks

PEG$_{s8}$-PLA-AL and PEG$_{s8}$-PLA-AM have been used to prepare crosslinked networks by the condensation of aldehyde and amine moieties to yield imine bonds (**Figure 3**a). At first, a model reaction was set up to confirm the formation of imine bonds between the selected aldehyde and amine derivatives (see details in the supporting data). Then, PEG$_{s8}$-PLA-AM and PEG$_{s8}$-PLA-AL were mixed in DCM to prepare films with a thickness ≈300 µm by solvent evaporation. In order to maximize the crosslinking efficiency but also to minimize the amount of residual free amine that could react with the polyester backbone, a ratio between aldehyde and amine chain-end moieties of 1:1 was selected. As the reaction is reversible, it is necessary to drive the aldehyde/amine equilibrium towards the imine formation by removing the water forming throughout the reaction (Figure 3b). Therefore, the crosslinking of the films was performed at 80 °C under vacuum for 24 h. By avoiding a prolonged heating at a temperature above 100 °C, undesirable amidation could be prevented.[29] Moreover, TGA analysis were carried out on the polymers and the results confirmed that no thermal degradation occurred at this temperature (Figures S4 and S5, Supporting Information).

The crosslinking of the network was evaluated by measuring gel fractions (GF) on samples after 24 hours of immersion in DCM and drying. The results are shown in the first line of **Table 2** and confirm a high crosslinking efficiency with a GF of 94.8 ± 0.6%. Moreover, a yellow color – characteristic of Schiff base formation[30] – appeared after crosslinking (Figure 3c,d).

Finally, the thermal properties of the crosslinked network were investigated. The sample exhibited a glass transition temperature of 15.5 °C (Table 2). As a consequence, and considering the foreseen applications as medical implants, a repair temperature of 37 °C was selected to allow chain mobility and therefore self-healing at physiological temperature.

Table 2. Gel fraction and glass transition temperature of the samples after different self-healing times. (Data are expressed as means ± SD and correspond to measurements with $n = 3$).

Self-healing time at 37 °C	Gel fraction [%]	*Tg* [°C]
undamaged material (control)	94.8 ± 0.6	15.5
5 min	95.6 ± 1.4	15.1
15 min	95.8 ± 0.5	15.5
30 min	94.5 ± 1.6	15.8
60 min	95.2 ± 0.8	15.5
120 min	94.4 ± 0.5	15.1

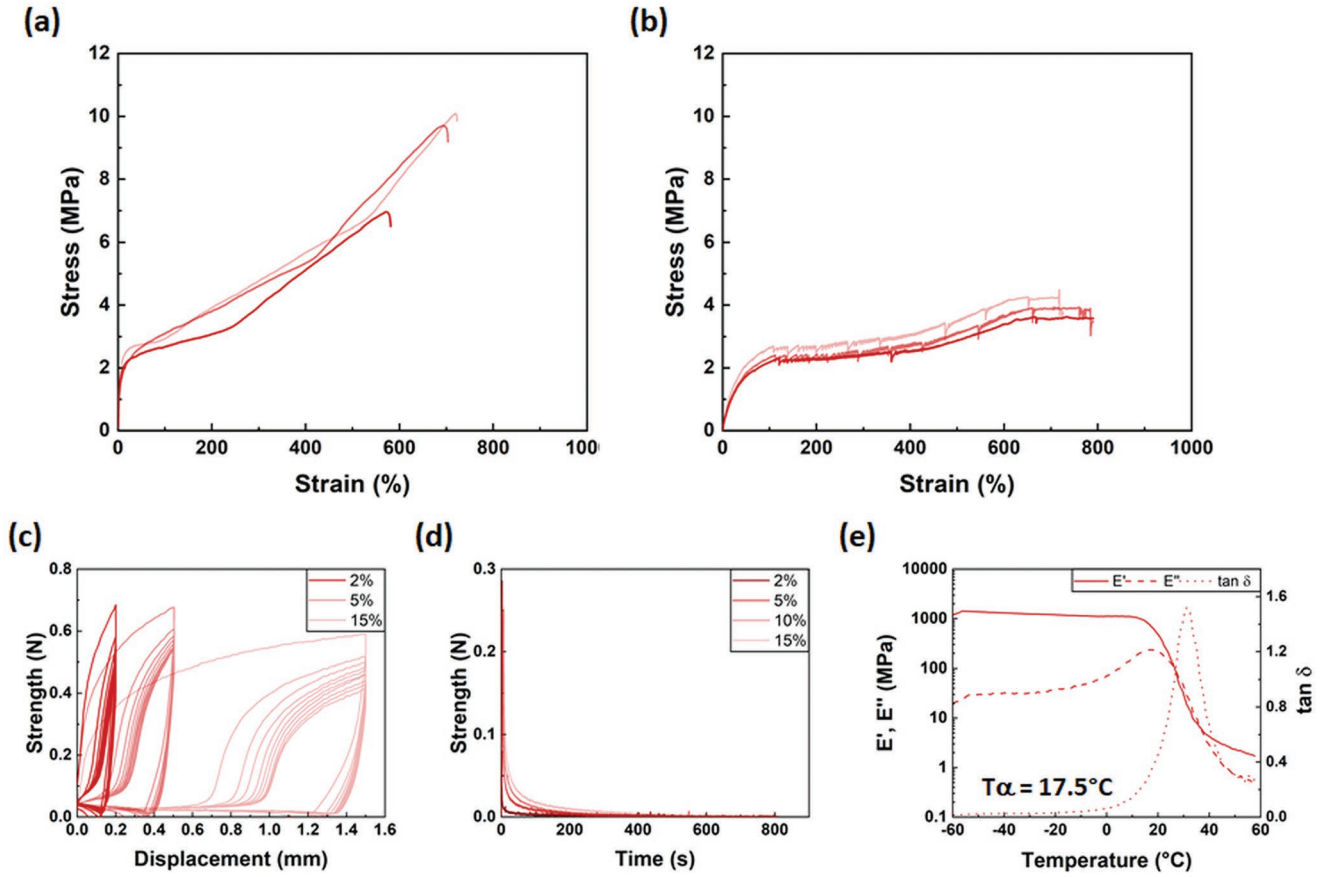

Figure 4. Evaluation of the mechanical properties of the imine-based network. Representative tensile curves a) in dry state at room temperature and b) in hydrated state at 37 °C. c) Cyclic load curves at 2,5 and 15% of deformation in dry state at room temperature. d) Relaxation curves at 2, 5, 10, and 15% of deformation in dry state at room temperature. e) Dynamic mechanical analyses.

3.3. Mechanical Properties of the Network

The mechanical properties of the crosslinked network based on imine bonds were first evaluated through uniaxial tensile test in a dry state at room temperature (**Figure 4**a). The test was also carried out in hydrated state at 37 °C to mimic physiological conditions (Figure 4b). The results are summarized in **Table 3**.

In the dry state and at room temperature, the imine-crosslinked network exhibited mechanical properties compatible with soft tissues (e.g., E of cartilage or skin[31]) and well above the ones of self-healable degradable hydrogels of the literature.[10] The material showed high strain ($\varepsilon_{break} = 714 \pm 110\%$) and stress at break ($\sigma_{break} = 9.4 \pm 2.2$ MPa) and Young's modulus reached 10.9 MPa. Nevertheless, the elastic domain was limited to 11 ± 1%. As expected, the mechanical properties decreased in the hydrated state at 37 °C. But interestingly, the new properties were still in the range of vascular tissues[31] with a Young's modulus and a stress at break of 4.4 ± 0.7 and 3.7 ± 0.2 MPa, respectively and increased elongation at break and elastic limit ($\varepsilon_{break} = 850 \pm 162\%$ and $\varepsilon_{yield} = 29 \pm 3\%$). Thus, the mechanical properties of the material are in accordance with the targeted applications in the biomedical field, as they are compatible with soft tissues of the human body. A point-to-point comparison with other systems of the literature is not easy as the polymers used are of various natures. However, our imine-based network displayed similar mechanical properties in terms of Young's modulus, strain, and stress at break compared to recently reported degradable self-healing elastomers for use in biomedical applications (Table S1, Supporting Information).

Cyclic tensile tests were also performed (Figure 4c). The material was submitted to nine cyclic loads at strain of 2, 5, and 15%. For the final cycle, the resilience was calculated and values of 35 ± 2, 28 ± 2, and 20 ± 1% were obtained, respectively.

The viscoelasticity of the networks was further characterized through relaxation tests. As shown in Figure 4d, the imine-crosslinked network displayed a viscous behavior with important relaxation within a few seconds. Whatever the strain (2, 5, 10, or 15%), the relaxation value reached 100% as expected for dynamic networks. Finally, DMA was carried out. The storage

Table 3. Mechanical properties in dry state at room temperature and in hydrated state at 37 °C of the imine-based network. (Data are expressed as means ± SD and correspond to measurements with $n = 3$).

	E [MPa]	σ_{yield} [MPa]	ε_{yield} [%]	σ_{break} [MPa]	ε_{break} [%]
Dry state, room temperature	10.9 ± 1.0	2.0 ± 0.2	11 ± 1	9.4 ± 2.2	714 ± 110
Hydrated state, 37 °C	4.4 ± 0.7	1.4 ± 0.1	29 ± 3	3.7 ± 0.2	850 ± 162

modulus of the material decreased from 1425 to 2 MPa with the increase of temperature from –60 to 60 °C (Figure 4e). A mechanical transition temperature ($T\alpha$) of 17.5 °C was determined. This temperature was close to the glass transition temperature (Tg) determined by DSC and below 37 °C, the temperature chosen for the self-healing process. Moreover, at 37 °C E' was higher than E'', which stresses out the more pronounced elastic nature of the network over its viscous component at this temperature which ensure shape stability after processing.

3.4. Self-Healing

The self-healing properties of the imine-based network were first investigated through visual shape recovery. The sample was cut into two halves, which were then reunited. The damaged sample was then heated at 37 °C and its ability to reform a single piece was assessed visually. As shown in **Figure 5**a, the material could heal in a single piece after 60 min. Moreover, the healed sample could not be broken through manual stretching (Movie S1, Supporting Information).

In order to quantify the self-healing properties, the recovery of the mechanical properties was then studied. Samples were cut before being slightly overlapped (contact area of 1 mm^2) and heated at 37 °C at different times (Figure 5b). The self-healing efficiency (SHE) was calculated by comparing the original values of strain and stress at break with those obtained after healing (Table S1, Supporting Information). As displayed in Figure 5c,d, the tensile properties were improved by increasing the self-healing time. The strain at break recovered significantly faster than the stress at break as shown by 82% for SHEε after only 30 min against 34% for SHEσ. This ultimately led to a full recovery of the strain at break after 60 min (SHEε = 107%; SHEσ = 77%), whereas it took twice that time for the stress at break (SHEε = 112%; SHEσ = 97%). The impact of the healing process at 37 °C on the crosslinking and thermal properties of the material was also assessed. Whatever the healing time, the values of GF and Tg remained like the one measured just after crosslinking on the undamaged sample (Table 2). It confirms that the extent of crosslinking in the network is not impacted by the healing process and that the network is stable under the conditions used.

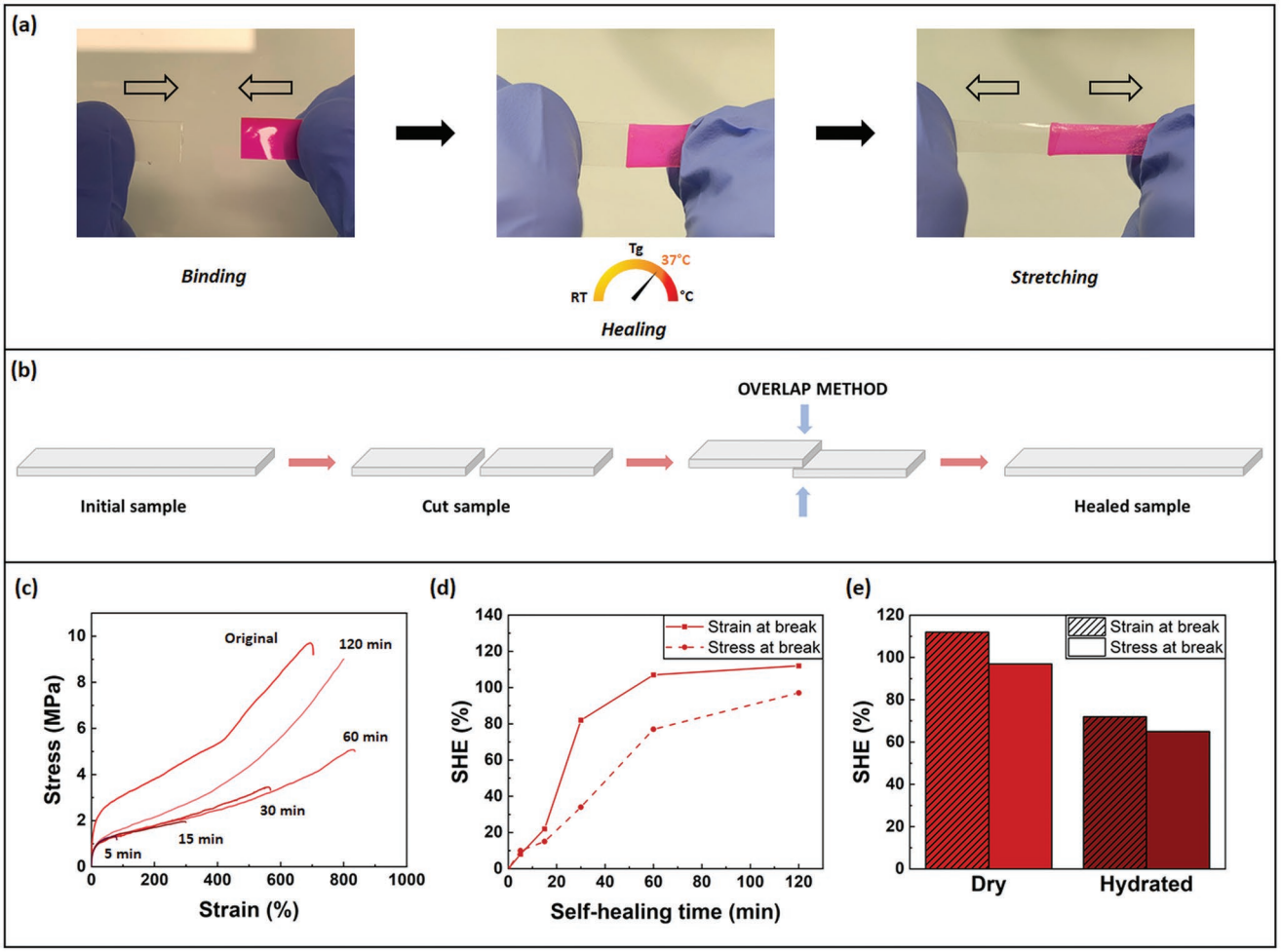

Figure 5. Evaluation of the self-healing properties of the imine-based network. a) Visual recovery. b) Schematic representation of the overlap method used to study the self-healing via the recovery of the mechanical properties. c) Tensile curves as a function of healing time in dry state. d) Evolution of SHE from 0 to 120 min at 37 °C in dry state. e) Comparison of SHE after 120 min of self-healing in dry and hydrated state.

Finally, the self-healing ability was also investigated in hydrated state and the results were compared with those obtained in dry state. After being cut and put together, the samples were immerged in PBS at 37 °C for 120 min. The tensile properties of the healed materials were then assessed in hydrated state at 37 °C (Table S2, Supporting Information) and compared to the original ones measured under the same conditions. Although diminished compared to dry state, the network showed remarkable abilities to self-repair in hydrated state with values of SHE of 72 and 65% for strain and stress at break, respectively after 120 min (Figure 5e).

Of notice, as imine-bond can be involved in various reversible reactions (Figure 1) it is difficult to determine which of them predominates in the self-healing process. However, we hypothesize that under the dry state self-healing is mainly due to transamination and imine metathesis reactions, whereas in the hydrated state the hydrolysis/condensation reaction can also play a role, which could explain the slightly lower SHE observed.

Overall, this set of results confirms that our imine-based network can self-heal under conditions that mimic physiological conditions (37 °C, dry or hydrated state), which is a great advantage for the development of self-healing systems intended for use in the biomedical field. This was an important challenge to tackle and it represents a clear advantage as many self-healable systems of the literature require self-healing conditions incompatible with biomedical applications, with for instance too high temperatures (Table S1, Supporting Information).

3.5. Preparation of 3D-Printed Scaffolds

3D-printing processing tests were then carried out. To obtain a homogenous mix of the two copolymers, PEG_{s8}-PLA-AM and PEG_{s8}-PLA-AL were first dissolved and stirred in DCM with a ratio of 1:1 between aldehyde and amine moieties. Then, the mixture was dried under vacuum and grinded to obtain a powder. The powder was then used to print 3D shapes. The mix of copolymers was easily processed using a 3D-Bioplotter equipment (Movie S2, Supporting Information) under relatively mild conditions (80 °C, 4 bar) and objects with good resolution could be obtained (**Figure 6**a). As mentioned previously, it was important to avoid heating at a temperature above 100 °C in order to prevent undesirable amidation and degradation of the polymer backbone.

Tubes of 1 cm in diameter and height were first printed at 80 °C (Figure 6b,c) before post-curing at the same temperature for 24 hours, which is largely above the glass transition temperature of the copolymers (*Tg* 15.5 °C). Therefore, to maintain the 3D shape the tubes were placed around a glass rod, which allowed them to preserve their design with limited creep (Figure 6d,e). This solution, although useful for the proof of concept shown here, could not be used for more complex shapes, which is a challenge to overcome in the frame of future developments.

The mechanical properties of the 3D-printed tubes were assessed through compression testing. Cyclic compression tests were first carried out in a dry state and room temperature. The samples were submitted to nine cyclic loads at strain of 2, 5, and 15%. The resilience was calculated for the final cycle and values of 50 ± 4, 39 ± 2, and 24 ± 4% were obtained, respectively. These values below 100% are characteristic of elastomeric networks and in accordance with those obtained in tensile mode, which confirmed that the 3D-printing process had no impact on the mechanical properties of the network. The compression set of the material was also evaluated in the same conditions to measure the permanent deformation that occurs when the tubes are compressed to a specific deflection. For a strain of 25%, the compression set reached 48 ± 1%, which indicates that the material was able to recover half of its uncompressed thickness. When the strain was decreased to 15%, a value of 17 ± 1% was obtained, which corresponds to over 80% of shape recovery. This demonstrates that when subjected to small deformations that are typical for blood vessels (e.g., < 10% for artery length and diameter during cardiac cycle[32]), the tubes show almost complete recovery.

Finally, to asset, an aspect that is rarely investigated in the literature,[10] the self-healing ability of the processed 3D-shaped biomaterials was evaluated (Movie S3, Supporting Information). To this end, a tube was connected to pipes, and a colored solution was injected. First, the liquid flowed through the undamaged tube without sign of leakage (**Figure 7**a). In a second step, a hole was punched in the tube with a needle to create a defect and a leak was clearly visible upon circulation of the solution (Figure 7b). To induce self-repair, the damaged tube was immersed in PBS and placed at 37 °C for 1 h in order to allow the repair under conditions that mimic physiological environment. After healing, the liquid was again able to circulate without leaking (Figure 7c), which demonstrates the potential of this material in the development of tubular scaffolds or other applications under physiological conditions.

3.6. Swelling Behavior and Degradation

Following the validation of their self-healing properties, the swelling and degradation of the network have been investigated.

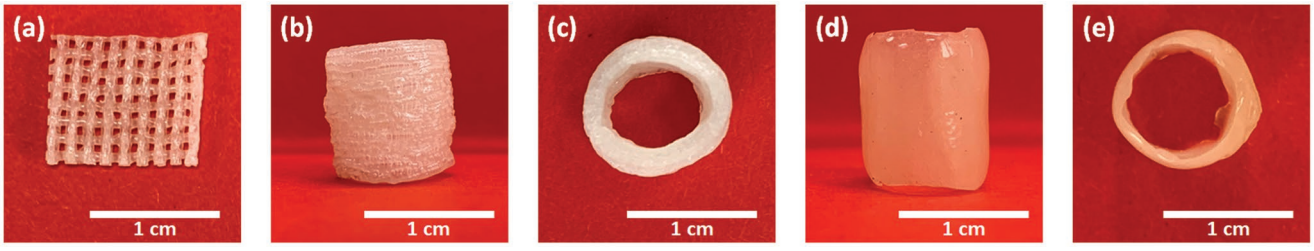

Figure 6. Pictures of 3D-printed devices with 3D-Bioplotter: a) grid, tube b,c) before and d,e) after cross-linking.

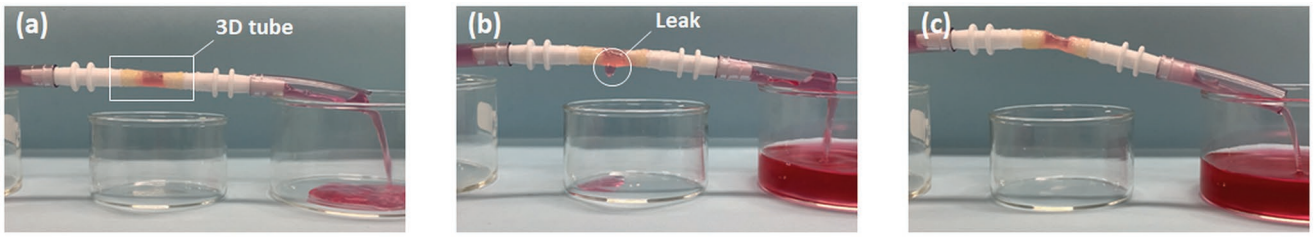

Figure 7. Pictures showing the passage of a colored solution in a tube made from the imine-crosslinked network a) before damage, b) after damage, and c) after healing.

As expected and due to the high amount of hydrophobic PLA in the copolymers (EG/LA = 0.4), the material showed a limited water uptake (44 ± 3%) after 4 days of immersion in PBS (**Figure 8**a).

The degradation of the network was studied over 2 months by monitoring the mass loss when immersed in PBS (pH 7.4) at 37 °C. The material showed a slow degradation with a remaining mass of 90 ± 2% after 60 days (Figure 8b). Different parameters can explain this result, such as the presence of chemical crosslinks, the large amount of hydrophobic PLA units in the network backbone, and the fact that imine hydrolysis is favored at acidic pH and not at pH 7.4.[33] Of notice, we can think that fast degrading networks would not require self-healing properties due to their rapid elimination and short lifetime. In opposition, this feature makes sense for slow degrading ones that would stay implanted for much longer periods of time.

3.7. Cytocompatibility

The potential of this imine-crosslinked network for use in cell-contacting applications was finally assessed. The cytotoxicity of the sample was first evaluated on extracts following ISO 10993-12 recommendations. The extracts from imine-crosslinked films or reference materials C+ and C- were added to L929 fibroblasts seeded into well, and cell viability was evaluated over a 24-hour

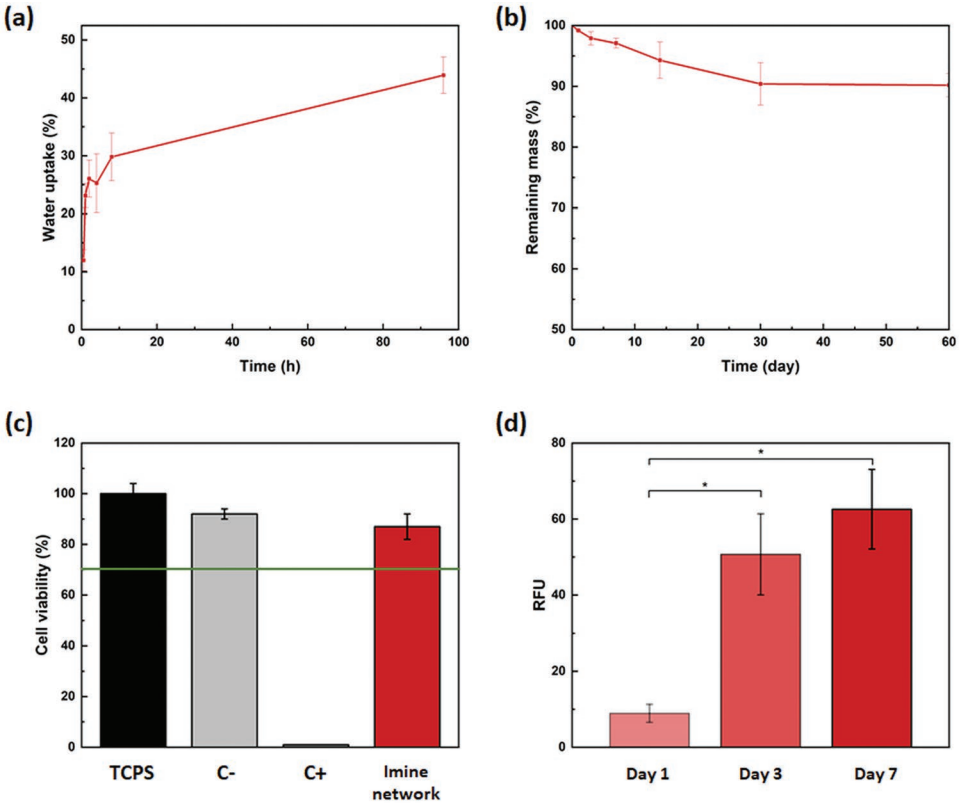

Figure 8. Degradation and cytocompatibility studies of the imine-based network. a) Evolution of water uptake in PBS (pH 7.4) with time. b) Evaluation of sample degradation in PBS at 37 °C. c) Cell viability evaluation assessed on L929 cells after treatment with an extract of polymer films for 24 h. Green line shows the 70% limit of viability considered in the ISO 10 993 standard. Data are expressed as means ± SD and correspond to measurements with $n = 3$. d) Proliferation of L929 cells on imine-crosslinked polymer films. Data are expressed as means ± SD and correspond to measurements with $n = 6$, $^*p < 0.05$.

period. Only extracts from positive control films (C+) gave 0% of viability on L929 cells. As shown in Figure 8c, the extract from the imine-based network induced viability of 87 ± 5%, which is above the 70% limit of the ISO 10 993 standard and highlights the noncytotoxicity of the sample. The proliferation of L929 cells on imine-crosslinked films was then evaluated over 7 days (Figure 8d). The noncytotoxicity of the material was also confirmed with fibroblasts cells being able to proliferate on the network. Overall, toxicity and proliferation assays confirm the absence of cell toxicity of this biomaterial and open the way for its future use in biomedical applications.

4. Conclusion

In this work, we designed a self-healable and degradable elastomeric network based on dynamic chemical bonds compatible with fused deposition modeling 3D-printing. Multi(aldehyde) star-shaped PEG_{s8}-PLA-AL and multi(amine) PEG_{s8}-PLA-AM were synthesized and used to obtain crosslinked networks through the condensation reaction between aldehyde and amine, which yields dynamic imine bonds providing self-healing abilities. The designed material is degradable, displays mechanical properties compatible with soft tissue applications, and shows quantitative self-healing properties. After full cut and 1 h recovery at 37 °C, the network shape was fully recovered and a high self-healing efficiency of 107 and 77% were obtained for the strain and stress at break, respectively. These values could even be further improved to 112 and 97% after 2 h. The material also displayed remarkable abilities to self-repair in hydrated state with values of SHE of 72% for strain and 65% for stress at break. The samples exhibited a slow mass loss over 2 months of degradation. The cytocompatibility of the network was demonstrated. Finally, this elastomeric material could be easily processed by fused deposition modeling 3D-printing in various shapes and was still able to self-heal after processing, under conditions compatible with biomedical applications. Overall these results demonstrate the potential of this new class of imine-based self-healable and degradable networks that could be used in the development of self-healable scaffolds for biomedical applications.

Supporting Information

Supporting Information is available from the Wiley Online Library or from the author.

Acknowledgements

This work was supported by the ANR2019-OPENN (ANR-19-CE19-0022-02) held by the University of Montpellier. The authors kindly acknowledge Mathieu Simon from the bio-impression platform CARTIGEN of the Institute for Regenerative Medicine and Biotherapy (IRMB) for the access to the 3D-printing equipment and the help with the 3D-printing process.

Conflict of Interest

The authors declare no conflict of interest.

Data Availability Statement

The data that support the findings of this study are available from the corresponding author upon reasonable request.

Keywords

3D-printing, degradable network, imine dynamic network, polyester, self-healing

Received: January 26, 2023
Revised: March 22, 2023
Published online: April 18, 2023

[1] Q. Chen, S. Liang, G. A. Thouas, *Prog. Polym. Sci.* **2013**, *38*, 584.
[2] C. Mangeon, E. Renard, F. Thevenieau, V. Langlois, *Mater. Sci. Eng. C* **2017**, *80*, 760.
[3] Y. Tu, N. Chen, C. Li, H. Liu, R. Zhu, S. Chen, Q. Xiao, J. Liu, S. Ramakrishna, L. He, *Acta Biomater.* **2019**, *90*, 1.
[4] S. Utrera-Barrios, R. Verdejo, M. A. Ló Pez-Manchado, M. Herná Ndez Santana, *Mater Horiz* **2020**, *7*, 2882.
[5] N. Roy, B. Bruchmann, J. M. Lehn, *Chem. Soc. Rev.* **2015**, *44*, 3786.
[6] L. Zhai, A. Narkar, K. Ahn, *Nano Today* **2020**, *30*, 100826.
[7] D. G. Bekas, K. Tsirka, D. Baltzis, A. S. Paipetis, *Composites, Part B Eng.* **2016**, *87*, 92.
[8] R. V. S. P. Sanka, B. Krishnakumar, Y. Leterrier, S. Pandey, S. Rana, V. Michaud, *Front. Mater.* **2019**, *6*, 137.
[9] D. L. Taylor, M. in h. Panhuis, *Adv. Mater.* **2016**, *28*, 9060.
[10] M. Grosjean, L. Gangolphe, B. Nottelet, *Adv. Funct. Mater.* **2023**, 2205315.
[11] R. Chang, Y. Huang, G. Shan, Y. Bao, X. Yun, T. Dong, P. Pan, *Polym. Chem.* **2015**, *6*, 5899.
[12] W. Ren, Z. Li, Y. Chen, H. Gao, W. Yang, Y. Wang, Y. Luo, *Macromol. Mater. Eng.* **2019**, *304*, 1800491.
[13] M. Wei, M. Zhan, D. Yu, H. Xie, M. He, K. Yang, Y. Wang, *ACS Appl. Mater. Interfaces* **2015**, *7*, 2585.
[14] Y. Wu, L. Wang, X. Zhao, S. Hou, B. Guo, P. X. Ma, *Biomaterials* **2016**, *104*, 18.
[15] S. Chen, X. Bi, L. Sun, J. Gao, P. Huang, X. Fan, Z. You, Y. Wang, *ACS Appl. Mater. Interfaces* **2016**, *8*, 20591.
[16] L. Zhang, J. Liang, C. Jiang, Z. Liu, L. Sun, S. Chen, H. Xuan, D. Lei, Q. Guan, X. Ye, Q. Guan, X. Ye, Z. You, *Natl Sci Rev* **2021**, *8*, https://doi.org/10.1093/nsr/nwaa154.
[17] M. Grosjean, L. Gangolphe, S. Déjean, S. Hunger, A. Bethry, F. Bossard, X. Garric, B. Nottelet, *ACS Appl. Mater. Interfaces* **2023**, *15*, 2077.
[18] H. Daemi, S. Rajabi-Zeleti, H. Sardon, M. Barikani, A. Khademhosseini, H. Baharvand, *Biomaterials* **2016**, *84*, 54.
[19] S. S. Rahman, M. Arshad, A. Qureshi, A. Ullah, *ACS Appl. Mater. Interfaces* **2020**, *12*, 51927.
[20] W. Q. Yuan, G. L. Liu, C. Huang, Y. D. Li, J. B. Zeng, *Macromolecules* **2020**, *53*, 9847.
[21] L. Zhang, Z. You, *Chin. J. Polym. Sci.* **2021**, *39*, 1281.
[22] C. Jiang, L. Zhang, Q. Yang, S. Huang, H. Shi, Q. Long, B. Qian, Z. Liu, Q. Guan, M. Liu, R. Yang, Q. Zhao, Z. You, X. Ye, *Nat. Commun.* **2021**, *12*, 4395.
[23] L. T. T. Nguyen, T. T. Truong, H. T. Nguyen, L. Le, V. Q. Nguyen, T. Van Le, A. T. Luu, *Polym. Chem.* **2015**, *6*, 3143.
[24] G. Rivero, L. T. T. Nguyen, X. K. D. Hillewaere, F. E. Du Prez, *Macromolecules* **2014**, *47*, 2010.
[25] H. Xuan, Q. Guan, H. Tan, H. Zuo, L. Sun, Y. Guo, L. Zhang, R. E. Neisiany, Z. You, *ACS Nano* **2022**, *16*, 16954.

[26] M. Ciaccia, S. Di Stefano, *Org. Biomol. Chem.* **2015**, *13*, 646.
[27] H. Li, J. Bai, Z. Shi, J. Yin, *Polymer* **2016**, *85*, 106.
[28] M. Grosjean, S. Ouedraogo, S. Déjean, X. Garric, V. Luchnikov, A. Ponche, N. Mathieu, K. Anselme, B. Nottelet, *ACS Appl. Mater. Interfaces* **2022**, *14*, 43719.
[29] R. L. Snyder, C. A. L. Lidston, G. X. De Hoe, M. J. S. Parvulescu, M. A. Hillmyer, G. W. Coates, *Polym. Chem.* **2020**, *11*, 5346.
[30] W. Kremers, J. W. Steele, *Can. J. Chem.* **1967**, *45*, 745.
[31] M. A. Meyers, P. Y. Chen, A. Y. M. Lin, Y. Seki, *Prog. Mater. Sci.* **2008**, *53*, 1.
[32] M. Niinomi, T. Narushima, M. Nakai, *Advances in Metallic Biomaterials: Tissues, Materials, and Biological Reactions*, Springer, Heidelberg **2015**.
[33] X. Qu, Z. Yang, *Chem. Asian J.* **2016**, *11*, 2633.